

Adsorption behavior of methylene blue on amine-functionalized ordered mesoporous alumina

Yiqun Gan · Na Tian · Xike Tian · Longlong Ma ·
Weiwei Wang · Chao Yang · Zhaoxin Zhou ·
Yanxin Wang

Published online: 13 November 2014
© Springer Science+Business Media New York 2014

Abstract Amine-functionalized ordered mesoporous alumina (NH₂-OMA) was synthesized through a facile and reproducible method. Its organic dyes adsorption characteristics, including adsorption isotherms, adsorption kinetics, the stability and reusability of the adsorbents were investigated. This material exhibited strong affinity to methylene blue and extremely high adsorption capacity. The maximum adsorption capacity value reached 657.89 mg g⁻¹. Adsorption kinetics was best described by the pseudo-second-order model. Equilibrium data were well fitted to the Langmuir isotherm model.

Keywords Mesoporous aluminium · Amine · Methylene blue · Adsorption

1 Introduction

Wastewaters from industries like textile, dyeing, printing, cosmetics, food coloring, papermaking, etc. are the major contributors of colored effluents [1, 2]. With the development of the dyeing and finishing industry, dye effluents have become one of the major sources of pollution, especially in China. The dye effluents may present high biotoxicity and potential mutagenic and carcinogenic effects [3–5].

Color is probably the only contaminant that could be recognized in water even at minute levels [6]. Color has to be removed from wastewater before discharging it into water bodies as it impedes light penetration and retards photosynthesis. The investigation on the removal of dyes from effluent wastewater of various industries has been going on for several years. There are three major technologies available to remove dyes from water (i.e., oxidation, adsorption, and flocculation-precipitation) [7–9]. Only recently membrane separation technology has been used for the separation of dyes from water. Among the oxidation methods, UV/ozone or UV/H₂O₂ is one of the best technologies for the total removal of dye from wastewater [10]. These methods are only effective for low concentrations of organic matter present in water. In other words, significant dilution of the water containing dye is necessary as a facility requirement for the effective use of the oxidation method. In the flocculation-precipitation process, the dye forms a complex with the flocculant [11]. Thus, the reuse of dye is impossible. At the same time, it can also lead to secondary pollution from the excessive use of coagulant compounds. The separation of dyes based on adsorption on clay [12, 13], activated carbon [14], agricultural waste biomass [15], and porous TiO₂-chitosan [16] have been proposed, and the adsorption kinetics have been studied in detail. These adsorption methods are capable of removing the dyes from concentrated wastewater. However, regeneration and separation of most of the adsorbents are difficult except for activated carbon. Thus, it is desirable to use the adsorption technique with new adsorbent materials for the removal of dyes from water that is simple, cost-effective, and permits reuse of the dyes.

Recently, mesoporous materials have attracted great interest as a new type of adsorbent for removing dyes, due to their remarkable features of the large specific surface

Y. Gan · X. Tian (✉) · Y. Wang
School of Environmental Studies, China University
of Geosciences, Wuhan 430074, People's Republic of China
e-mail: xktian@cug.edu.cn

N. Tian · X. Tian · L. Ma · W. Wang · C. Yang · Z. Zhou
Faculty of Materials Science and Chemistry, China University
of Geosciences, Wuhan 430074, People's Republic of China

area, large and tunable pore channels, such as mesoporous silica, mesoporous carbon, and mesoporous alumina [17–20]. Chemical modifications of the pore with metals, metal oxides, and organic moieties are successful in tailoring the physical and chemical properties of these materials. Eftekari et al. [21] reported modification of MCM-41 by incorporation of aluminum can enhance adsorptive of MB. Ho et al. [22] have shown that amino- and carboxylic-functionalized MCM-41 are effective adsorbents for the removal of Acid blue 25 and Methylene blue from water. Polyelectrolyte-functionalized mesoporous silica was proved to be potent adsorbents for anionic dye in an aqueous solution [23]. The adsorption properties of surface-functionalized mesoporous adsorbents have been successfully prepared and shown to have remarkable adsorption capacity [24–26].

Herein, we present an easily accessible, reproducible, and high-throughput method to synthesize highly ordered mesoporous amine-functionalized alumina via in situ sol-gel reactions with NH_4NO_3 as amine source. Methylene blue (MB), a water-soluble cationic dye, was used as a target contaminant to characterize the adsorptive properties of the amine-functionalized mesoporous alumina. Models to fit the adsorption equilibrium and kinetic data were presented.

2 Experimental

2.1 Materials

Pluronic P123 ($\text{EO}_{20}\text{PO}_{70}\text{EO}_{20}$) was purchased from Aldrich. Aluminum iso-propoxide, HCl, ethanol and NH_4NO_3 were purchased from Shanghai Nanxiang Reagent Co., Ltd., China. All chemicals were analytical grade and used without further purification. MB supplied by Zhongyuan Chemical Co., LTD (Beijing, china) selected for adsorption test.

2.2 Synthesis of amine-functionalized ordered mesoporous alumina

The amine-functionalized ordered mesoporous alumina (NH_2 -OMA) was prepared according to our previous method with some modification [27–29]. In a typical synthesis, 1 g of pluronic P123 was dissolved in 12 mL of ethanol to obtain a absolute solution A. In solution B, 1.5 mL of 37 wt% hydrochloric acid was added dropwise in 6 mL of ethanol, and 2.04 g of aluminum iso-propoxide as precursor was portioned slowly to solution B under vigorous stirring at 40 °C. Then solution B was blended with the solution A. To this mixture, 3 g of NH_4NO_3 was added as amine source. The resulting mixture was stirred at

40 °C water bath to form a clear sol, and further the homogeneous sol was aging for 3 days at 40 °C. The solution was put into a 60 °C drying oven to undergo the solvent evaporation process. Finally, the resultant amino-functionalized mesoporous alumina was obtained by calcining the as-prepared samples at 400 °C for 4 h in air. The additional synthesis of ordered mesoporous alumina without modified was similar to that described above, in which NH_4NO_3 was not been used.

2.3 Characterization

TEM were taken on the JEOL 2000 EX transmission electron microscope under a working voltage of 200 kV. The nitrogen adsorption and desorption isotherms at 78.3 K were measured using an ASAP 2020 analyzer (Micromeritics Co. Ltd., USA). The pore size distributions were derived from the desorption branches using the Barrett–Joyner–Halenda (BJH) model. FTIR spectra were recorded on a Nicolet Avatar 370 DTGS spectrometer. The leached Al concentration in the supernatant was determined by an Aanalyst 800 atomic absorption spectroscopy (AAS, Perkin-Elmer Corporation, America).

2.4 MB adsorption experiments

Batch adsorption experiments were carried out at 25 ± 1 °C in a thermostated shaker. At first, aqueous solutions containing different concentrations of MB (20 – 180 mg L^{-1}) were prepared. The initial pH of solutions was adjusted to about 7 by the addition of NaOH and HCl solution. Then adsorption kinetics and adsorption isotherms were studied separately. For the adsorption kinetics tests, 0.01 g adsorbents were added to 50 mL of MB (100 mg L^{-1}) solutions under stirring, and stirring was continued for a predetermined equilibrium time intervals. To study the adsorption isotherms, 0.01 g adsorbents were put into the flasks containing 50 mL of MB solution of different initial concentrations (20 – 180 mg L^{-1}). The flasks were kept in an isothermal shaker for 24 h to reach equilibrium of the solution and solid mixture. At last, after adsorption process, the mixture of liquid and solid were separated by centrifugation to measure the concentrations of MB solution. The measurements of MB concentrations were carried out using a UV–Vis spectrophotometer. The amount of MB retained in the sorbent phase (mg g^{-1}) was obtained according to Eq. (1):

$$q_e = \frac{(C_i - C_e)V}{m} \quad (1)$$

where C_i and C_e are the initial and final (equilibrium) concentration of the MB in solution (mg L^{-1}), V is the solution volume (L), and m is the mass of sorbent (g).

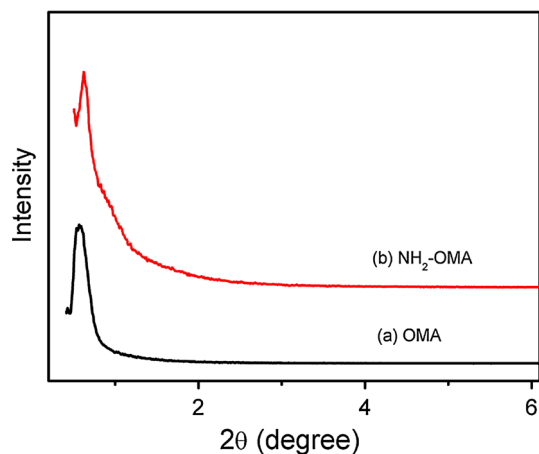


Fig. 1 Small-angle X-ray diffraction (SAXRD) patterns for OMA (a) and NH₂-OMA (b)

2.5 Regeneration

The regeneration of NH₂-OMA containing MB was investigated by a chemical desorption method. A certain amount of adsorbents were added into the flasks having the MB solution (100 mg L⁻¹) to be adsorbed and agitated in a thermostated shaker at 25 °C for a certain time until reaching equilibrium. The leached MB concentrations were determined by a UV–Vis spectrophotometer. After adsorption process, the collected adsorbents containing MB was added to 100 mL NaOH solution (1 mol L⁻¹) under stirring using isothermal shaker. After removing NaOH solution, the adsorbent was washed with 0.5 mol L⁻¹ acetic acid solutions and deionized water. Then it was dried at 60 °C. The regenerated adsorbent was further used for adsorption/desorption test. The adsorption/desorption process was cycled five times.

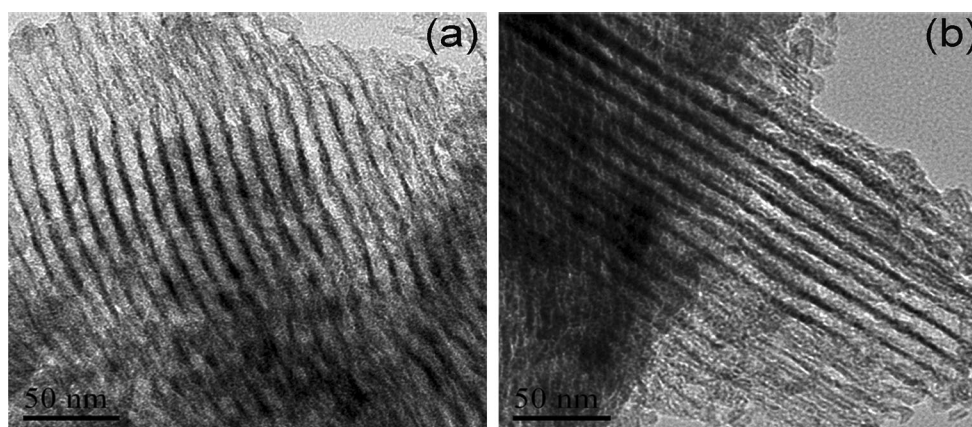


Fig. 2 TEM images of OMA (a) and NH₂-OMA (b)

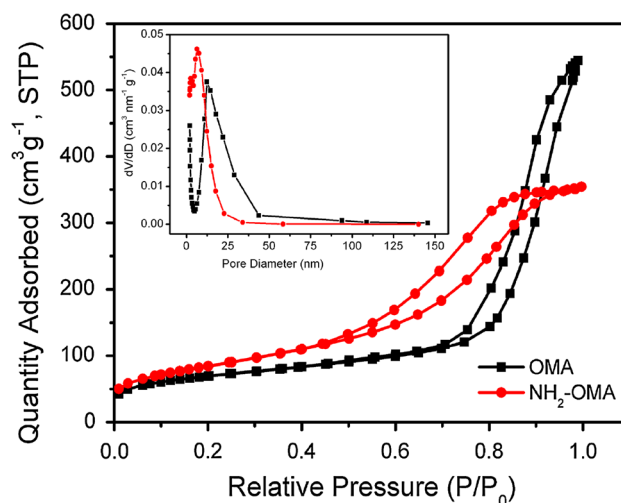


Fig. 3 Nitrogen adsorption–desorption isotherms and pore size distributions (*inset*) of OMA and NH₂-OMA

3 Results and discussion

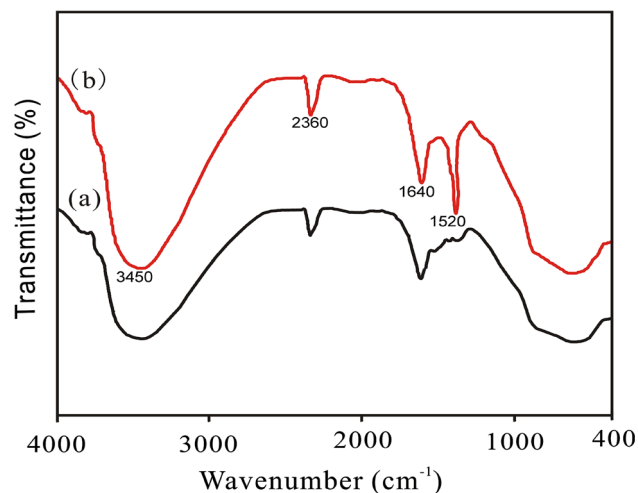
3.1 Characterization of NH₂-OMA

Evidence for the formation of mesostructures is provided by small-angle X-ray diffraction patterns shown in Fig. 1. The samples of OMA and NH₂-OMA show a very strong diffraction peak around 0.6°, which confirms the high degree of ordering. The ordered mesoporous structure can be observed by TEM images (Fig. 2). TEM images confirm a hexagonally packed pore structure along with uniform channels over a large area, suggesting a long-range ordered mesostructure.

The nitrogen adsorption–desorption isotherms (Fig. 3) of OMA and NH₂-OMA yield type IV curves with H1-shaped hysteresis loops, suggesting their uniform cylindrical pores

Table 1 Structural parameters of the OMA, NH₂-OMA samples

Sample	S _{BET} (m ² g ⁻¹)	Pore volumes (cm ³ g ⁻¹)	Pore size (nm)
OMA	248.2	0.7954	12.82
NH ₂ -OMA	305.4	0.5423	7.102

**Fig. 4** FT-IR spectra of OMA (a) and NH₂-OMA (b)

[30]. This is consistent with TEM electron microscopy results. The amine-functionalized mesoporous alumina has a large BET surface area of 305.47 m² g⁻¹ and a pore volume of 0.5423 cm³ g⁻¹. Amine modified mesoporous alumina has a smaller pore diameter of about 7.1 nm. The adsorption parameters for the samples studied are summarized in Table 1. Narrow pore-size distributions are maintained though the diameter decreases when amino functional groups are grafted onto the ordered mesoporous alumina. The large surface area, large and tunable pore channels, and narrow pore-size distribution enhance its adsorption capacity of dyes since dyes are bulky molecules with sizes of over 1 nm.

FT-IR spectra of OMA and NH₂-OMA are illustrated in Fig. 4. The NH₂-OMA characteristic peaks (due to –NH₂ and –OH groups stretching vibrations at 3,450 cm⁻¹) are partially obscured by adsorbed water. For the –NH₂ identification only could be considered the N–H for primary amine band at 1,520 cm⁻¹. Adsorptions at 3,450 and 1,640 cm⁻¹ are attributed to –NH₂ and –OH groups stretching vibrations in the NH₂-OMA [31, 32]. A schematic illustration of aminated process is described in Fig. 5. The aminated reaction occur involving two schemes as follow. Firstly, most of supported NH₄NO₃ is decomposed to ammonia in the process of calcination. Then, ammonia can be immobilized or

incorporated onto the surface of OMA frameworks and reacted with the limited Al–OH, which is similar to the process of nitridation reaction on the mesoporous silicon oxynitride materials [33].

3.2 Adsorption kinetics

To determine the time necessary to get access to equilibrium adsorption, the effect of contact time on adsorption of MB onto NH₂-OMA was studied at the initial concentrations 100 mg L⁻¹. Figure 6 shows the effect of contact time on the adsorption of MB on NH₂-OMA and OMA. It can be seen that a rapid adsorption of MB by NH₂-OMA occurred, with equilibrium reached in approximately 40 min for NH₂-OMA. It was particularly noteworthy that the process showed an extraordinarily high uptake of MB, which can be verified by the fact that the amount of adsorbed MB onto NH₂-OMA within 40 min achieved 498.10 mg g⁻¹.

In order to further understand the characteristics of the adsorption process, the pseudo-first-order and pseudo-second-order kinetic models were applied to fit experimental data obtained from batch experiments. The pseudo-first-order and pseudo-second-order kinetic models are expressed in linear form as follows [34]:

$$\ln(q_e - q_t) = \ln q_e - K_1 t \quad (2)$$

$$\frac{t}{q_t} = \frac{1}{K_2 q_e^2} + \frac{t}{q_e} \quad (3)$$

where q_e and q_t (mg g⁻¹) are the amounts of MB adsorbed at equilibrium and at time t (min), respectively. K_1 (min⁻¹) is the pseudo-first-order rate constant and K_2 (g mg⁻¹ min⁻¹) is the pseudo-second-order rate constant. The kinetic parameters and the correlation coefficients (R^2) were determined by linear regression (Fig. 7) and were given in Table 2. The calculated q_e values ($q_{e,cal}$) of the pseudo-second-order kinetic model is close to the experimental ones ($q_{e,exp}$), and the plots show quite good linearity with R^2 above 0.9999. Therefore, the adsorption kinetics follows the pseudo-second-order model well, suggesting a chemisorption process.

The Weber's intraparticle diffusion model was further employed to identify the steps involved during adsorption process [35], which is described as:

$$q_t = k_i t^{1/2} + C \quad (4)$$

where k_i is the intraparticle diffusion rate constant (mg g⁻¹ min^{-1/2}), C is a constant (mg g⁻¹). From the plots of q_t versus $t^{1/2}$ for various dyes, multilinearities are observed in Fig. 8a, implying that more than one process affects the adsorption. The initial region is a diffusion adsorption stage, attributing to the diffusion of dye through

Fig. 5 Schematic depiction of preparing process of NH₂-OMA

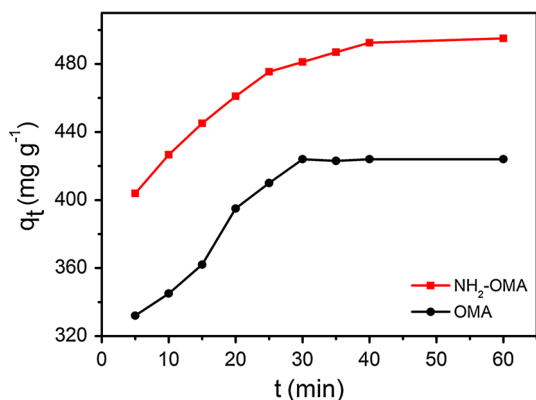
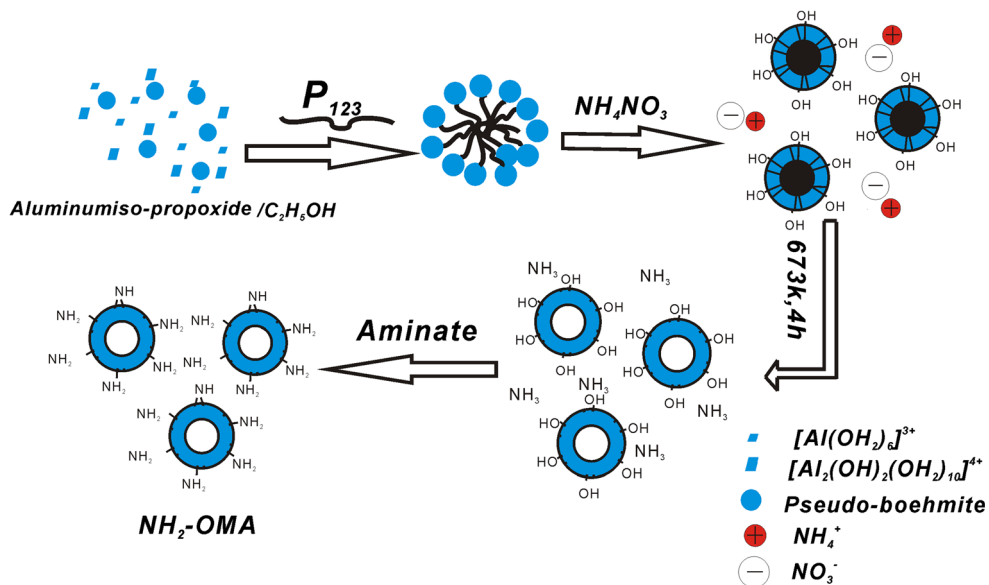


Fig. 6 Adsorption rate curves for MB: circles are for OMA; squares are for NH₂-OMA

the solution to the external surface of adsorbent (external diffusion). The second region is a gradual adsorption stage, corresponding to intraparticle diffusion of dye molecules through the pores of adsorbent (intraparticle diffusion).

Therefore, both film diffusion and intraparticle diffusion processes are simultaneously operating MB adsorption onto NH₂-OMA. The observed multilinearity also suggests that intraparticle diffusion is not the rate-limiting step. The values of k_i and C were calculated from the slope and intercept of plots of q_t versus $t^{1/2}$ (Fig. 8a) and were summarized in Table 3.

To establish the actual rate-controlling step involved in the MB adsorption processes, the adsorption kinetic data are further fitted using the Boyd kinetic model [36], which is expressed as:

$$F = 1 - \frac{6}{\pi^2} \exp(-B_t) \tag{5}$$

where F is the fraction of solute adsorbed at different time t and B_t is a mathematical function of F and is given by

$$F = \frac{q_t}{q_e} \tag{6}$$

Fig. 7 a Pseudo-first-order and b pseudo-second-order kinetics for MB adsorption on NH₂-OMA

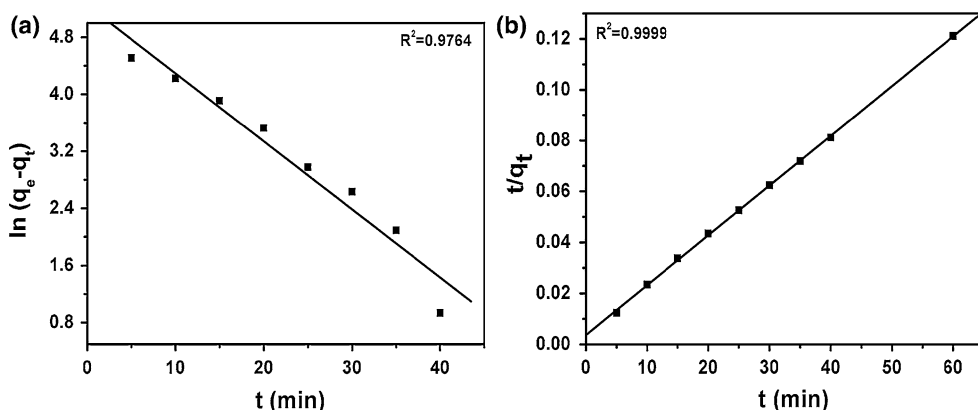
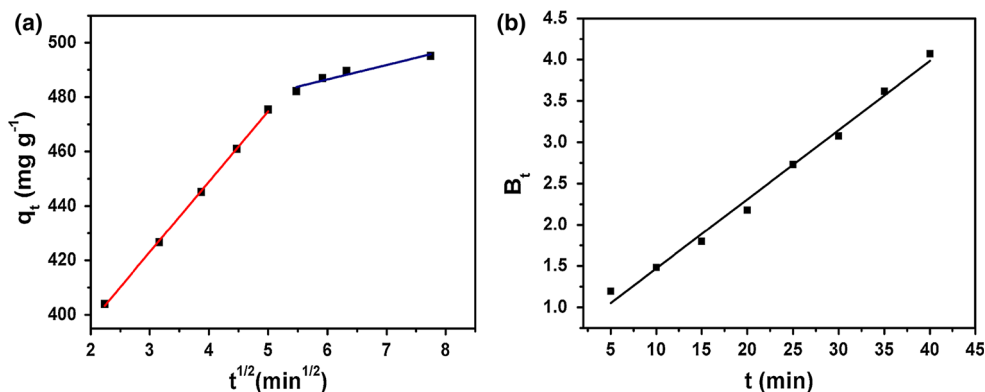


Table 2 Kinetic parameters for adsorption of MB on NH₂-OMA

C_0 (mg L ⁻¹)	$q_{e, exp}$ (mg g ⁻¹)	First-order kinetic model			Second-order kinetic model		
		$q_{e, cal}$ (mg g ⁻¹)	K_1 (min ⁻¹)	R^2	$q_{e, cal}$ (mg g ⁻¹)	K_2 (g mg ⁻¹ min ⁻¹)	R^2
100	498.10	190.3	0.0954	0.9764	510.2	0.0011	0.9999

Fig. 8 **a** Intraparticle diffusion plots for the adsorption of MB onto NH₂-OMA; **b** Boyd plots for the adsorption of MB onto NH₂-OMA**Table 3** Intraparticle diffusion model parameters and Boyd model parameters for the adsorption of MB onto the NH₂-OMA

C_0 (mg L ⁻¹)	Intraparticle diffusion model						Boyd model	
	$K_{i,1}$ (mg g ⁻¹ min ^{-1/2})	C_1 (mg g ⁻¹)	R^2	$K_{i,2}$ (mg g ⁻¹ min ^{-1/2})	C_2 (mg g ⁻¹)	R^2	B_t (Linear)	R^2
100	24.67	349.27	0.9976	3.74	466.57	0.8678	$B_t = 0.4577 + 0.0954t$	0.9764

Table 4 Comparison of the adsorption capacities of MB onto various adsorbents

Adsorbent	Maximum adsorption capacities	Reference
Activated carbon	454.2 mg g ⁻¹	[5]
AIMCM-41	0.208 mmol g ⁻¹	[21]
Carboxylic-containing functional groups onto MCM-41	223 mg g ⁻¹	[22]
Halloysite nanotubes	84.32 mg g ⁻¹	[26]
MTZ/imogolite	0.6513 mmol g ⁻¹	[41]
Highly-ordered mesoporous SBA-15	0.154 mmol g ⁻¹	[42]
Titania nanotubes	290 mg g ⁻¹	[43]
NH ₂ -OMA	657.89 mg g ⁻¹ (2.06 mmol g ⁻¹)	This work

Substitution of Eq. (5) in Eq. (6), the kinetic expression can be represented as

$$B_t = -0.4977 - \ln\left(1 - \frac{q_t}{q_e}\right) \quad (7)$$

Figure 8b shows the plot modeled by the Boyd kinetic model. It shows that the plot is linear but don't pass through the origin. The R^2 value of linear fitting is 0.9764, indicating that the film diffusion is the rate-controlling step in the MB adsorption on NH₂-OMA processes (Table 4).

3.3 Adsorption isotherms

The equilibrium adsorption isotherm is indispensable in describing the interaction between pollutant and adsorbent. Figure 9a typically shows the adsorption isotherms of MB onto NH₂-OMA at 25 °C. It was observed that the equilibrium adsorption capacity q_e , increased with an initial steep rise followed by slight elevation to a more or less plateau promptly along with the increase of equilibrium concentration. The explicit isotherm of L-shape, according

Fig. 9 **a** Adsorption isotherm for the adsorption MB onto NH₂-OMA; **b** effect of initial concentration on the adsorption of MB onto NH₂-OMA

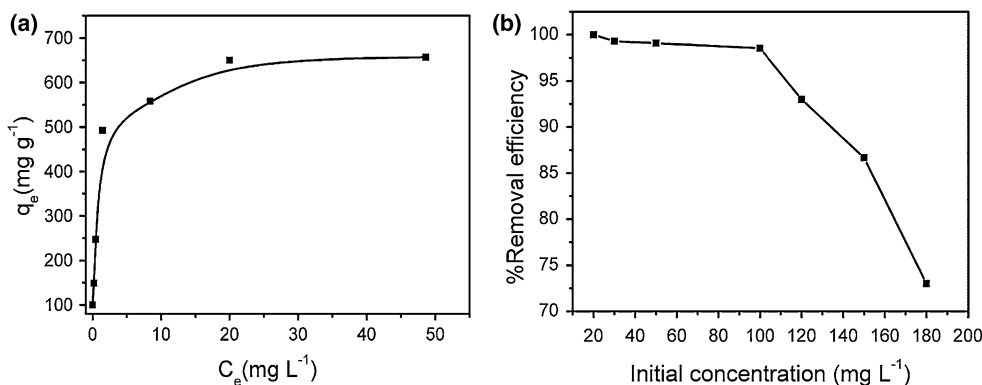
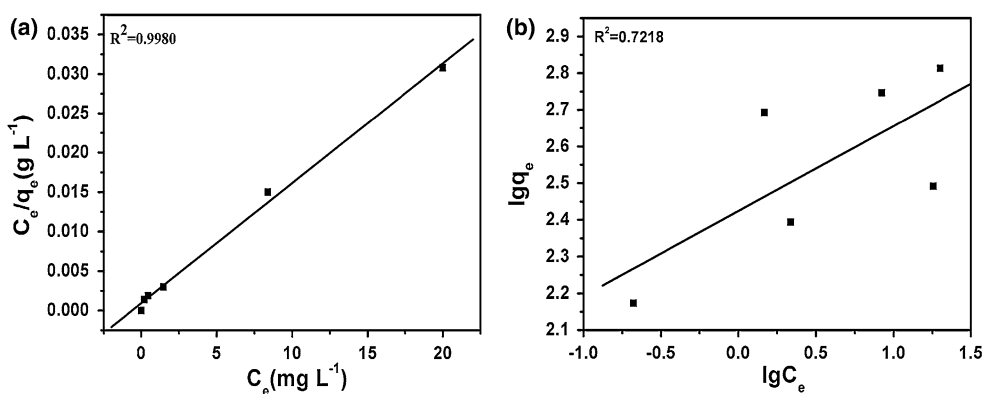


Fig. 10 **a** Langmuir adsorption isotherms and **b** Freundlich adsorption isotherms for the adsorption MB onto NH₂-OMA



to Giles et al. [37], indicated that there was no strong competition between the solvent and the dye to occupy the NH₂-OMA active sites. Moreover, this type of isotherm implies Langmuir-type adsorption between MB and NH₂-OMA molecules. With the increase of initial MB concentration from 20 to 180 mg L⁻¹, the amount of the adsorbed MB at equilibrium increased from 100 to 657.01 mg g⁻¹. The experimental results also showed a decrease of MB removal at equilibrium condition. The removal percentage dropped from 100 to 73 % (Fig. 9b) when the initial concentration rose from 20 to 180 mg L⁻¹. This was due to fast saturation on the surface of NH₂-OMA as MB concentration was increased, leading to the decrease of adsorption efficiency. The fact that the removal percentage was higher at lower concentration showed that the available adsorbent surface area was the key factor to achieve high adsorption efficiency.

To further describe the equilibrium adsorption isotherm, the Langmuir isotherm and Freundlich isotherm models were used for test study [38, 39]. Langmuir isotherm assumes monolayer adsorption onto a surface containing a finite number of adsorption sites of uniform strategies of adsorption with no transmigration of adsorbate in the plane of surface. However, Freundlich isotherm model assumes heterogeneous surface energies, in which the energy term in Langmuir equation varies as a function of the surface

coverage. The applicability of the isotherm equation is compared by judging the correlation coefficients, R². Both isotherm models are represented as follow:

$$\frac{C_e}{q_e} = \frac{1}{K_L q_{max}} + \frac{C_e}{q_{max}} \tag{8}$$

$$\lg q_e = \frac{1}{n} \lg C_e + \lg K_f \tag{9}$$

where C_e (mg L⁻¹) is the equilibrium concentration of MB in solution, q_e (mg g⁻¹) is the amount of MB adsorbed per unit weight of adsorbent at equilibrium, q_{max} and K_L are Langmuir constants related to the adsorption capacity and rate of adsorption, respectively. K_f and n are Freundlich constants with n giving an indication of how favourable the adsorption process and K_f is the adsorption capacity of the adsorbent. The isotherms based on the experimental data and the parameters obtained from linear regression by both models are shown in Fig. 10. The R² values of Langmuir and Freundlich models are 0.9979 and 0.7128, respectively, indicating that the Langmuir model is suitable for describing the adsorption equilibrium of MB onto NH₂-OMA. The monolayer adsorption capacity determined from the Langmuir isotherm is 657.89 mg g⁻¹. Table 3 compares the adsorption capacity of NH₂-OMA obtained in this study with different adsorbents previously used for removal of MB from aqueous solutions. The adsorption

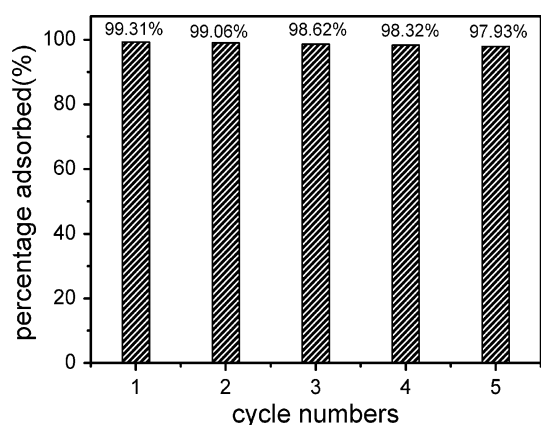


Fig. 11 Reusability of NH₂-OMA adsorbent (initial concentration of the MB: C₀ = 100 mg/L)

capacity of MB onto NH₂-OMA is higher than that of many other previously reported adsorbents, suggesting that the as-prepared NH₂-OMA has great potential application in dye removal from aqueous solution. And, the major mechanism of MB adsorption onto the NH₂-OMA was electrostatic interaction.

The essential characteristics of Langmuir isotherm can be expressed by a dimensionless constant called separation factor or equilibrium parameter (R_L), defined by Weber and Chakkravorti as follow:

$$R_L = \frac{1}{1 + K_L C_0} \quad (10)$$

The obtained R_L values at different initial MB concentration were in the range of 0.9765–0.9970, which lie between 0 and 1, confirming that the adsorption of MB on the NH₂-OMA was favourable at the conditions being studied.

3.4 Stability and reusability of the adsorbents

The stability and regeneration ability of the adsorbent is crucial for its practical application. Considering that component leaching from adsorbent to water environment may cause secondary pollution, the stability of the NH₂-OMA composite was tested by monitoring the leached Al content. In this case, no leaching of Al ions from the NH₂-OMA was detected during MB adsorption at natural pH by AAS, indicating the high stability of NH₂-OMA. S. Asuha has reported that MO saturated on mesoporous TiO₂ can be successfully regenerated using sodium hydroxide [40]. To further evaluate the performance of the adsorbent, the same reuse experiments were carried out. The regenerated and recycled results of NH₂-OMA (Fig. 11) indicate that the fading rate for the MB solution was almost unaffected even after the fifth run with regenerated adsorbent. This behavior indicates that the adsorbent can be easily recovered and

recycled efficiently and thus NH₂-OMA has the potential for application in industry.

4 Conclusion

In conclusion, amine-functionalized ordered mesoporous alumina has been successfully synthesized by a facile sol-gel method. Adsorption ability of the NH₂-OMA is evaluated by choosing the methylene blue as an adsorbate. The present study shows that the NH₂-OMA, with the high surface area of 305.47 m² g⁻¹, has great adsorption capacities of MB. Adsorption kinetics follows the pseudo-second-order model. The adsorption process is operated by both film diffusion and intraparticle diffusion, and the film diffusion is determined to be the rate-controlling step. Equilibrium data are fitted by Langmuir and Freundlich isotherms and the equilibrium data are better described by Langmuir isotherm model, with maximum monolayer adsorption capacity of 657.89 mg g⁻¹. The NH₂-OMA has large pore channels with pore diameter of about 7.1 nm, which improves its adsorption capacity of dyes since dyes are bulky molecules with sizes of over 1 nm. The high surface area, large pore channels and electrostatic attraction between NH₂-OMA and MB account for the high adsorptive performance of the NH₂-OMA. Therefore, the NH₂-OMA is an economical and efficient sorbent and it will have potential applications for removing residual dyes from waste waters.

Acknowledgments This work was supported by the National Basic Research Program of China (973 Program, Grant No. 2011CB933700) of the Ministry of Science and Technology of China, the National Natural Science Foundation of China (Grant Nos. 51371162 and 51344007) and the Fundamental Research Funds for the Central Universities.

References

1. M. Ertaş, B. Acemioğlu, M.H. Alma, M. Usta, J. Hazard. Mater. **183**, 421 (2010)
2. Y. Xie, D. Qian, D. Wu, X. Ma, Chem. Eng. J. **168**, 959 (2011)
3. N. Bao, Y. Li, Z. Wei, G. Yin, J. Niu, J. Phys. Chem. C **115**, 5708 (2011)
4. C. Chen, P. Gunawan, R. Xu, J. Mater. Chem. **21**, 1218 (2011)
5. B.H. Hameed, A.T.M. Din, A.L. Ahmad, J. Hazard. Mater. **141**, 819 (2007)
6. Y.C. Pei, J.J. Wang, X.P. Xuan, J. Fan, M. Fan, Environ. Sci. Technol. **41**, 5090 (2007)
7. L. Ai, C. Zhang, F. Liao, Y. Wang, M. Li, L. Meng, J. Jiang, J. Hazard. Mater. **198**, 282 (2011)
8. J. Ma, Y.Z. Jia, Y. Jing, J.H. Sun, Y. Yao, X.H. Wang, J. Hazard. Mater. **175**, 965 (2010)
9. M. Srinivasan, T. White, Environ. Sci. Technol. **41**, 4405 (2007)
10. Y.C. Hsu, Y.F. Chen, J.H. Chen, J. Environ. Sci. Heal. A **39**, 127 (2004)
11. T.H. Kim, C. Park, J.M. Yang, S. Kim, J. Hazard. Mater. **112**, 95 (2004)

12. A. Xue, S. Zhou, Y. Zhao, X. Lu, P. Han, J. Hazard. Mater. **194**, 7 (2011)
13. S. Hong, C. Wen, J. He, F. Gan, Y.S. Ho, J. Hazard. Mater. **167**, 630 (2009)
14. R. Sandoval, A.M. Cooper, K. Aymar, A. Jain, K. Hristovski, J. Hazard. Mater. **193**, 296 (2011)
15. V.J.P. Vilar, C.M.S. Botelho, R.A.R. Boaventura, J. Hazard. Mater. **147**, 120 (2007)
16. C.E. Zubieta, P.V. Messina, C. Luengo, M. Dennehy, O. Pieroni, P.C. Schulz, J. Hazard. Mater. **152**, 765 (2008)
17. S. Wang, H. Li, Micropor. Mesopor. Mater. **97**, 21 (2006)
18. X. Zhuang, Y. Wan, C. Feng, Y. Shen, D. Zhao, Chem. Mater. **21**, 706 (2009)
19. Y.H. Kim, C.M. Kim, I.H. Choi, S. Rengaraj, J.H. Yi, Environ. Sci. Technol. **38**, 924 (2004)
20. K. Lee, S.W. Park, M.J. Ko, K. Kim, N.G. Park, Nat. Mater. **8**, 665 (2009)
21. S. Eftekhari, A. Habibi-Yangjeh, S. Sohrabnezhad, J. Hazard. Mater. **178**, 349 (2010)
22. K.Y. Ho, G. McKay, K.L. Yeung, Langmuir **19**, 3019 (2003)
23. J.B. Joo, J. Park, J. Yi, J. Hazard. Mater. **168**, 102 (2009)
24. S.M. Grant, A. Vinu, S. Pikus, M. Jaroniec, Colloid. Surface. A **38**, 121 (2011)
25. Q. Qin, J. Ma, K. Liu, J. Hazard. Mater. **162**, 133 (2009)
26. M. Zhao, P. Liu, Micropor. Mesopor. Mater. **112**, 419 (2008)
27. Z.Z. Wang, X.K. Tian, C. Yang, Y.X. Zhao, Z.B. Pi, J. Nanosci. Nanotechnol. **12**, 6876 (2009)
28. C. Yang, L.L. Gao, Y.X. Wang, X.K. Tian, S. Komarneni, Micropor. Mesopor. Mater. **197**, 156 (2014)
29. X.K. Tian, Q.Y. Wu, K.M. Wong, C. Yang, W.W. Wang, X.N. Wu, Y.X. Wang, S.X. Zhang, Y. Lei, Appl. Surf. Sci. **284**, 412 (2013)
30. S.M. Morris, P.F. Fulvio, M. Jaroniec, J. Am. Chem. Soc. **130**, 15210 (2008)
31. J.C. Wang, Q. Liu, Micropor. Mesopor. Mater. **83**, 225 (2005)
32. X. Wang, X. Liu, L. Lai, S. Li, J. Weng, Z. Zhou, Q. Cui, X. Chen, M. Cao, Q. Zhang, Adv. Funct. Mater. **18**, 1809 (2008)
33. Y.D. Xia, R. Mokaya, Angew. Chem. Int. Edit. **42**, 2639 (2003)
34. X.P. Liao, B. Shi, Environ. Sci. Technol. **39**, 4628 (2005)
35. M. Dogan, H. Abak, M. Alkan, J. Hazard. Mater. **164**, 172 (2009)
36. G.E. Boyd, A.W. Adamson, L.S. Meyers, J. Am. Chem. Soc. **69**, 2836 (1947)
37. C.H. Giles, T.H. MacEwan, S.N. Makhwa, D. Smith, J. Chem. Soc. **56**, 3973 (1960)
38. I. Langmuir, J. Am. Chem. Soc. **38**, 2221 (1916)
39. H.M.F. Freundlich, J. Phys. Chem. **57**, 385 (1906)
40. S. Asuha, X.G. Zhou, S. Zhao, J. Hazard. Mater. **181**, 204 (2010)
41. D.L. Guerra, A.C. Batista, R.R. Viana, C. Airoidi, J. Hazard. Mater. **183**, 81 (2010)
42. C.H. Huang, K.P. Chang, H.D. Ou, Y.C. Chiang, C.F. Wang, Micropor. Mesopor. Mater. **141**, 102 (2011)
43. C.T. Hsieh, W.S. Fan, W.Y. Chen, Micropor. Mesopor. Mater. **116**, 677 (2008)